The Astrophysical Journal Letters, 899:L6 (12pp), 2020 August 10 https://doi.org/10.3847/2041-8213/aba907

A Comparative Study of Host Galaxy Properties between Fast Radio Bursts and Stellar Transients

Ye Li[1,2] and Bing Zhang[3]
[1] Kavli Institute for Astronomy and Astrophysics, Peking University, Beijing 100871, People's Republic of China; liye_kiaa@pku.edu.cn
[2] Purple Mountain Observatory, Chinese Academy of Sciences, Nanjing 210008, People's Republic of China
[3] Department of Physics and Astronomy, University of Nevada, Las Vegas, NV 89154, USA
Received 2020 May 5; revised 2020 July 22; accepted 2020 July 24; published 2020 August 6

Abstract

Recent arcsecond localizations of fast radio bursts and identifications of their host galaxies confirmed their extragalactic origin. While FRB 121102 resides in the bright region of a dwarf star-forming galaxy, other FRBs reside in more massive galaxies and are related to older stellar populations. We compare the host galaxy properties of nine FRBs with those of several types of stellar transients: from young to old populations, long-duration gamma-ray bursts (LGRBs), superluminous supernovae (SLSNe), SNe Ibc, SNe II, SNe Ia, and short-duration gamma-ray bursts (SGRBs). We find that the stellar mass and star formation rate of the FRB host galaxies, taken as a whole sample, prefer a medium to old population, and are against a young population, similar to LGRBs and SLSNe by a null probability of 0.02. Individually, the host of FRB 121102 is consistent with that of young population objects; the environment of FRB 180924 is similar to that of SGRBs; and the environment of FRB 190523 is similar to those of SNe Ia. These results are consistent with the magnetar engine model for FRBs, if magnetars produced from extreme explosions (GRBs/SLSNe) and those from regular channels (e.g., those producing Galactic magnetars) can both produce FRBs.

Unified Astronomy Thesaurus concepts: Radio transient sources (2008)

1. Introduction

Fast radio bursts are extragalactic radio transients with durations of 0.01–50 ms and dispersion measures (DMs) in excess of the Galactic values (Lorimer et al. 2007; Cordes & Chatterjee 2019; Petroff et al. 2019). More than 100 FRBs have been reported (FRBCAT,[4] Petroff et al. 2016). While most are one-off bursts, at least 20 sources show repeating bursts (e.g., Scholz et al. 2016; Spitler et al. 2016; CHIME/FRB Collaboration et al. 2019a, 2019b; Kumar et al. 2019; Fonseca et al. 2020; Luo et al. 2020). More than 50 theoretical models have been proposed (see Katz 2016; Platts et al. 2019 for theoretical reviews[5]). Most models invoke neutron stars or other compact objects (e.g., black holes or white dwarfs) as the sources.

Thanks to observations with the Karl G. Jansky Very Large Array, the Deep Synoptic Array ten-antenna prototype (DSA-10), the European VLBI Network, and the Commensal Real-time ASKAP Fast Transients Survey (ASKAP/CRAFT), the arcsecond localization data of nine FRB sources have been published. These include the repeating sources FRB 121102 (Chatterjee et al. 2017) and FRB 180916.J0158+65 (Marcote et al. 2020) and apparently non-repeating sources FRB 180924 (Bannister et al. 2019), FRB 181112 (Prochaska et al. 2019), FRB 190523 (Ravi et al. 2019), FRB 190102, FRB 190608, FRB 190611, and FRB 190711 (Bhandari et al. 2020; Macquart et al. 2020). In the field of gamma-ray bursts (GRBs), multi-wavelength properties, especially the host galaxy properties, have played an important role in identifying two physically distinct classes of sources, i.e., long GRBs (LGRBs) due to core collapse of massive stars and short GRBs (SGRBs) due to mergers of binary neutron stars (e.g., Fruchter et al. 2006; Fong et al. 2010; Berger 2014; Blanchard et al. 2016; Li et al. 2016). For FRBs, the host galaxy properties and the location of the FRB source within the galaxies also carry clues to diagnose their possible origin(s).

The properties of the FRB host galaxies so far indicate a perplexing picture. FRB 121102, the first repeater and the first FRB localized with arcsecond precision, resides in the brightest region of a star-forming dwarf galaxy (Bassa et al. 2017; Chatterjee et al. 2017; Kokubo et al. 2017; Tendulkar et al. 2017), whose properties are quite similar to those of the host galaxies of young stellar population transients, e.g., LGRBs and superluminous supernovae (SLSNe). This observation motivated the suggestion that young magnetars produced from these extreme explosions are the sources of repeating FRBs (e.g., Murase et al. 2016; Beloborodov 2017; Metzger et al. 2017), and it was predicted that the majority of FRBs should reside in similar environments (e.g., Nicholl et al. 2017). However, later precise localizations of other FRBs suggest otherwise. For example, FRB 180924, FRB 190523, and FRB 180916.J0158+65 are located in massive galaxies. Furthermore, FRB 180924 resides far away from the center of its host. These properties are similar to those of the host galaxies of old population transients, such as SGRBs (Bannister et al. 2019; Ravi et al. 2019). This may point toward an origin of FRBs related to compact binary coalescences (e.g., Totani 2013; Margalit et al. 2019; Wang et al. 2020; Zhang 2020).

It is possible that FRBs are not related to the extremely young or extremely old stellar populations. If this is the case, then neither LGRBs/SLSNe nor SGRBs are good population proxies for FRBs. It is also possible that the observed FRBs may include subclasses with diverse origins, as most other astrophysical phenomena do. Indeed, the FRB host properties seem to be diverse given the limited information available (Li et al. 2019). In order to make an assessment of the origin of FRBs based on their host galaxy data, it is essential to collect

[4] http://www.frbcat.org/, updated to 2019 December 23.
[5] https://frbtheorycat.org/index.php/Main_Page

the statistical properties of the host galaxies of different types of stellar transients and compare the FRB host properties with them.

In this paper, we carry out such a task. Besides LGRBs/SLSNe and SGRBs, which represent the youngest and oldest stellar populations, we also perform a statistical analysis of the host galaxies of intermediate stellar transients. From young to old, they are LGRBs, SLSNe, SNe Ibc, SNe II, SNe Ia, and SGRBs. We compare the host properties between FRBs and these transients, trying to address the following questions: Which host galaxy type are the FRB hosts more analogous to as a whole or individually? Could there be diverse origins of FRBs? We construct the paper as follows. The host galaxy samples of different types of transients are presented in Section 2. The host galaxy properties of FRBs are compared with those of different types of stellar transients as a whole in Section 3.1 and individually in Section 3.2. The implications of our results are discussed in Section 4. The cosmological parameters $H_0 = 67.8\,\mathrm{km\ s^{-1}\ Mpc^{-1}}$, $\Omega_\mathrm{m} = 0.308$, and $\Omega_\Lambda = 0.692$ are adopted (Planck Collaboration et al. 2016).

2. Parameters and Samples

We discuss the parameters considered in this paper in Section 2.1 and present the samples of FRBs and various transients in Section 2.2.

2.1. Parameters

Our goal is to compare the host galaxy properties of FRBs with those of other transients. The properties of the host galaxies can be documented in a set of parameters, both the global properties on the galactic scale and the local properties on the sub-galactic scale. We discuss these parameters in turn.

2.1.1. Galactic-scale Parameters: $\log \mathrm{M}_*$, SFR, Metallicity, R_{50}

The most important global properties of the host galaxies are stellar mass M_*, star formation rate SFR, specific star formation rate sSFR (SFR/M_*), metallicity $12 + \log(\mathrm{O/H})$, as well as the half-light radius R_{50} of the host galaxies. The stellar mass M_* of a galaxy is usually estimated by fitting the broadband spectral energy distribution (SED) to the stellar population synthesis (Arnouts et al. 1999; Kauffmann et al. 2003; Boquien et al. 2019). Star formation rate is estimated from emission lines such as Hα, or ultraviolet (UV) luminosity (see Kennicutt & Evans 2012 for a review). sSFR is estimated as SFR/M_* when SFR and M_* are both available. The transients related to younger populations (LGRBs and SLSNe) are more likely to reside in the galaxies with smaller stellar masses and more intense SFR and sSFR (and sometimes less metallicity) than those related to old populations (Kelly et al. 2008; Schulze et al. 2018). The metallicity of a galaxy is usually estimated from its emission (Kewley & Dopita 2002; Kobulnicky & Kewley 2004; Pettini & Pagel 2004; Kewley & Ellison 2008; Dopita et al. 2016) or absorption line ratios (Draine 2011). The emission line method gives metallicity in the form of $12 + \log(\mathrm{O/H})$, with the solar metallicity being $12 + \log(\mathrm{O/H})_\odot = 8.69$ (Asplund et al. 2009). The absorption line method, on the other hand, gives metallicity in the form of $[\mathrm{X/H}] = \log(N_\mathrm{X}/N_\mathrm{H}) - \log(N_\mathrm{X}/N_\mathrm{H})_\odot$, where N_X indicates the column density of element X. To be consistent, we convert $12 + \log(\mathrm{O/H})$ to [X/H] in this paper. For metallicities estimated from emission lines, we choose to use those estimated based on Dopita et al. (2016) when available, to be consistent with that estimated for FRB 180916.J0158+65.

The half-light radius R_{50} is the radius that encloses 50% of the total light of the galaxy. It is usually estimated by fitting the surface brightness of a galaxy with the Sérsic profile

$$\Sigma(r) = \Sigma_\mathrm{e} \exp\{-k_\mathrm{n}[(r/r_\mathrm{e})^{1/n} - 1]\},$$

where the effective radius r_e represents R_{50}. Another way is to fit the brightness profiles with ellipses centered around the galaxy and identify the one whose enclosed flux is half of the total flux. R_{50} is defined as the semimajor axis of the ellipse. In general, R_{50} scales with stellar mass M_*. For the same stellar mass, a star-forming galaxy usually has a larger R_{50} than a passive galaxy.

2.1.2. Sub-galactic Parameters: R_{off}, r_{off}, F_{light}

The same galaxy may host different types of transients. Thus, local properties at the sub-galactic level can provide more precise diagnostics to the environment of a certain transient. One important property is the offset of the transient from the center of the host galaxy. It can be measured in physical units (kiloparsecs) as R_off, or normalized to the characteristic radius of the host $r_\mathrm{off} = R_\mathrm{off}/R_{50}$. The larger R_off, the farther away the transient is from the center of the host, and the fainter and more quiescent the local environment is. However, R_off is misleading for irregular galaxies since the center of the galaxy is hard to define and usually does not mark the region with most intense star formation. For these cases, F_light is a more efficient parameter. It is defined as the total light emitted in the region fainter than the transient position, within the host. By definition, a transient within the brightest region would have $F_\mathrm{light} \sim 1$, and one within the faintest region would have $F_\mathrm{light} \sim 0$ (Fruchter et al. 2006; Anderson et al. 2015a, 2015b).

For a nearby transient, surface brightness Σ, local color, and local star formation rate density Σ_SFR would give more precise information. However, these parameters are not available for most objects at larger distances. Since the redshifts of the localized FRBs are in the range 0–1, a valid local star formation rate density Σ_SFR is hard to obtain for most of them. We therefore use galaxy-scale properties M_*, SFR, sSFR, [X/H], and R_{50}, and sub-galactic scale properties R_off, $r_\mathrm{off} = R_\mathrm{off}/R_{50}$, and F_light in this study.

2.2. Samples of FRBs and Stellar Transients

Different types of transients show somewhat different properties in both global galactic and sub-galactic features (Fruchter et al. 2006; Kelly et al. 2008; Anderson et al. 2012; Kelly & Kirshner 2012; Li et al. 2016). Comparing the properties of FRBs with those of other transients can shed light on the origin of FRBs. In the following, we discuss the samples of FRBs and other transients used in our study.

2.2.1. Fast Radio Bursts

We summarize the host galaxy properties of the FRBs studied in this paper in Table 1. For FRB 180916.J0158+65, the global SFR is scaled from that at the FRB position as $\mathrm{SFR} = 0.016 \times 6.57/1.002 = 0.1\ M_\odot\ \mathrm{yr}^{-1}$. The metallicity of FRB 180916.J0158+65 is estimated based on Dopita et al. (2016). We then choose to use the metallicity values based on

Table 1
Host Galaxy Properties of FRBs with Host Galaxies Identified

	Instrument	z	log SFR	log sSFR	log M_*	[X/H]	R_{50}	Offset	Offset	$F_{\rm light}$	References
			($M_\odot$ yr^{-1})	(Gyr^{-1})	($M_\odot$)		(kpc)	(kpc)	(R_{50})		
FRB 121102	Arecibo	0.19273	−0.40	0.86	7.7	−0.59	1.4	0.82	0.60	1.0	1
FRB 180916.J0158+65	CHIME/FRB	0.0337	−1.0	−2.0	10.0	0.13	3.3	4.7	1.5	⋯	5, 7
FRB 180924	ASKAP	0.3214	<0.30	<−2.0	10.3	⋯	2.8	3.8	1.4	0.08	3
FRB 181112	ASKAP	0.4755	−0.22	−0.62	9.4	⋯	3.9	$3.1^{+15.7}_{-3.1}$	0.79	⋯	4, 6
FRB 190102	ASKAP	0.2913	0.18	−0.33	9.5	−0.25	5.3	$1.5^{+3.4}_{-1.5}$	0.28	⋯	6
FRB 190523	DSA-10	0.66	<0.11	<−2.0	11.1 ± 0.1	−0.52	⋯	$26.5^{+15.5}_{-14.9}$	⋯	⋯	2
FRB 190608	ASKAP	0.11778	0.079	−1.3	10.4	−0.34	⋯	6.8 ± 1.3	⋯	⋯	6
FRB 190611	ASKAP	0.378	⋯	⋯	⋯	⋯	⋯	17.2 ± 4.9	⋯	⋯	8
FRB 190711	ASKAP	0.522	⋯	⋯	⋯	⋯	⋯	$1.5^{+3.6}_{-1.5}$	⋯	⋯	8

References. (1) Tendulkar et al. (2017); (2) Ravi et al. (2019); (3) Bannister et al. (2019); (4) Prochaska et al. (2019); (5) Ahumada et al. (2020); (6) Bhandari et al. (2020); (7) Marcote et al. (2020); (8) Macquart et al. (2020).

the same reference for FRB 121102 as well as for other transients when available. The half-light radius R_{50} of FRB 180916.J0158+65 is not available from the paper. We estimate R_{50} with the Petrosian half-light radius $R_{50,\rm petro} = 4\farcs66$ and the 90% radius as $R_{90,\rm petro} = 8\farcs53$ from the Sloan Digital Sky Survey (SDSS) catalog, using the formula $R_{50} = R_{50,\rm petro}/(1 - 8 \times 10^{-6}(R_{90,\rm petro}/R_{50,\rm petro})^{8.47}) = 4\farcs7$ (Graham et al. 2005). This gives a physical distance of 3.3 kpc. We estimate the offset of FRB 190523 with the coordinates (J2000) of the FRB, right ascension (R.A.) 13:48:15.6(2), declination (decl.) +72:28:11(2), and the host coordinates from the PanSTARRS, stack R.A. 13:48:15.426 (207.°06427), decl. +72:28:14.6 (72.°47072). The offset is estimated to be $3.7^{+2.2}_{-2.1}$ arcsec, corresponding to $26.5^{+15.5}_{-14.9}$ kpc for its redshift. Note that the astrometric registration between FRB 190523 and the Pan-STARRS image is not available here, which may result in an additional ∼(0.″3–0.″5) uncertainty.

The metallicities from Bhandari et al. (2020) are provided as Z. They are converted to [X/H] by using $[{\rm X/H}] = \log_{10}(Z/Z_\odot)$, where $Z_\odot = 0.0196$ is the solar metallicity.

In summary, seven well localized FRBs have stellar mass, SFR, and sSFR available. All of the nine FRBs have offset information available. Note that while FRB 121102, FRB 180916.J0158+65, FRB 180924, FRB 190608, and FRB 190611 have well defined offsets, the offsets of FRB 181112, FRB 190102, and FRB 190711are consistent with being zero. Although the localization of FRB 190523 is relatively poor, a relatively large offset is favored.

2.2.2. Samples of LGRBs and SGRBs

Li et al. (2016) compiles 407 GRBs with redshifts or host galaxy properties from the literature (e.g., Fruchter et al. 2006; Fong et al. 2010; Berger 2014; Blanchard et al. 2016 and references therein), with all the estimation methods labeled. The stellar mass (M_*) values of Li et al. (2016) are mainly obtained from SED fitting by Savaglio et al. (2009) and Leibler & Berger (2010), but some are estimated from the K-band or infrared (IR) magnitudes. Due to the large uncertainty of the latter method, only those estimated with SED fitting are included in this study. The SFR values collected in Li et al. (2016) are mainly estimated with emission lines from Savaglio et al. (2009), Krühler et al. (2015), and Berger (2009), with some estimated using UV fluxes. The emission lines usually trace recent star formation (<10 Myr), related to LGRBs, while the UV fluxes trace 10–200 Myr star formation, related to core-collapse SNe (see Kennicutt & Evans 2012 for a review). Thus, we use the SFR values estimated using both methods. The metallicity values collected in Li et al. (2016) are estimated with both emission line ratios (Kobulnicky & Kewley 2004; Pettini & Pagel 2004; Kewley & Ellison 2008; Savaglio et al. 2009; Krühler et al. 2015) and absorption line ratios (Draine 2011; Cucchiara et al. 2015). If the metallicity [X/H] is estimated with $R_{23} = ([{\rm O\,II}]\ \lambda3727 + [{\rm O\,III}]\ \lambda\lambda4959, 5007)/{\rm H}\beta$, the results are double-valued from Kewley & Ellison (2008) and from Savaglio et al. (2009). In this case, we only select the larger value of the two, following Kobulnicky & Kewley (2004) and Berger (2009). The half-light radius R_{50} of the host galaxy and the offset of the GRB from the center of the host are mainly derived from Hubble Space Telescope (HST) images (Bloom et al. 2002; Wainwright et al. 2007; Fong et al. 2010; Fong & Berger 2013; Blanchard et al. 2016). Usually galaxies are inclined. The offsets are sometimes corrected for the inclination. However, the statistical results are not influenced significantly by the inclinations of the objects (Japelj et al. 2018). All the FRB and GRB offsets are projected offsets. To be consistent, we also use projected offsets in the SN section. See Li et al. (2016) for more details.

Here we only use the well measured parameters, with upper and lower limits excluded. Following Li et al. (2020), here we do not include the four GRBs whose physical categories are subject to debate, i.e., GRB 060505, GRB 060614, GRB 090426, and GRB 060121. The numbers of LGRBs and SGRBs with host galaxy properties are 263 and 31, respectively. To make the GRB sample more consistent with that of FRBs, we only use LGRBs and SGRBs with redshifts $z < 1$ for comparison. This results in smaller sample sizes, i.e., 72 LGRBs and 22 SGRBs.

2.2.3. Samples of SLSNe, SNe Ibc, SNe II, and SNe Ia

For SNe, we use the data from the Open Supernovae Catalog (OSC)[6] as the starting point to build our samples. The OSC includes the coordinates (R.A. and decl.) of the SNe and the names and coordinates of their hosts. Some host galaxies in the OSC do not have coordinates labeled. For these, we search for their names in SIMBAD[7] to collect their coordinates. To be

[6] https:sne.space
[7] http://simbad.u-strasbg.fr/simbad/sim-fid

consistent, all available host galaxy names and coordinates are calibrated to SIMBAD IDs and coordinates. Some host galaxies are not available in SIMBAD. They are calibrated to NED[8] instead. In order to reduce the misidentification of the host galaxies, we exclude those SNe with host galaxy distances larger than 1°. We then collect the host galaxy information from the papers exploring SNe and galaxy catalogs.

Properties from SN papers—We first supplement the host galaxy properties from the papers exploring the SN host galaxy properties. We match their SN names with the OSC names or aliases during this process.

For the stellar mass, we use the values estimated with SED fitting only. For SFR, we prefer those estimated by emission lines, especially Hα. If this is not available, we use the value estimated using the far-ultraviolet (FUV) method. When no value from the above two methods is available, we use the SFR value derived from the SED fitting. Kelly & Kirshner (2012) estimated the stellar mass using SED fitting, sSFR using fiber spectra, and metallicity using emission lines and the method of Pettini & Pagel (2004, hereafter PP04) for different types of transients. Taggart & Perley (2019) and Schulze et al. (2018) estimated the stellar mass and SFR of core-collapse supernovae and SLSNe using SED fitting. For SLSNe only, Perley et al. (2016) estimated log M_* and SFR using SED fitting and estimated the SFR with emission lines when spectra are available. For SNe Ia, more than 600 log M_*, SFRs, and metallicities are produced using SED fitting by Kim et al. (2018).

For metallicity, we prefer those values estimated using the emission line method, especially those based on PP04 and Dopita et al. (2016, hereafter D16). To be consistent with FRB 180916.J0158+65, whose host metallicity was estimated with D16, we adopt those from D16 whenever available. Otherwise, the values from PP04 are adopted. Graham (2019) estimated the SN host metallicities and provided the largest SN sample estimated with D16. Kelly & Kirshner (2012), Schady et al. (2019), and Anderson et al. (2016) estimated metallicities with the PP04 method for various transients. For SNe Ia located in passive galaxies, Kang et al. (2016, 2020) estimated the host metallicities using absorption line ratios. We use those [M/H] values based on the Yonsei evolutionary population synthesis models (Chung et al. 2013).

We prefer the half-light radius R_{50} estimated using 2D Sérsic fitting. Lunnan et al. (2015) and Japelj et al. (2018) provided R_{50} in the r band for SLSNe and SNe Ic-BL, respectively. Other R_{50} values of SN hosts are obtained from galaxy catalogs.

The offsets $R_{\rm off}$ between SNe and their hosts are usually available from the OSC. However, the offsets are sometimes not trustworthy, because the R.A. of the host galaxies in the Asiago SN catalog is accurate to seconds, with an uncertainty of 15″. These are not suitable for offset calculations. We thus extract the host galaxy coordinates from the SDSS-II catalog (Sako et al. 2018), the ASAS-SN catalog,[9] and the bright SN catalog[10] by matching the OSC SN names with the names in other catalogs. In our analysis, the offsets for the FRB sample as well as the OSC and GRB samples are not corrected for inclination. We therefore use the projected offsets whenever available. We also update the offset values from the detailed papers exploring SN offsets. In particular, Anderson et al. (2016) and Japelj et al. (2018) provided the projected $R_{\rm off}$. Kelly & Kirshner (2012) gave the deprojected $r_{\rm off}$.

The $F_{\rm light}$ values are compiled from the papers exploring SN properties. Anderson et al. (2012) calculated $F_{\rm light}$ in both Hα and near-UV bands for various SNe transients. Hα traces on-going star formation (0–16 Myr), which is more relevant to LGRBs, and near-UV traces recent star formation (16–100 Myr) (Gogarten et al. 2009), which is more relevant to core-collapse supernovae. However, $F_{\rm light}$ values for Hα are usually not available for relatively high redshifts. We thus employ the $F_{\rm light}$ for near-UV whenever available. Anderson et al. (2015a) and Lunnan et al. (2015) provided $F_{\rm light}$ values from UV for SNe Ia and SLSNe, respectively. Kelly et al. (2008) estimated $F_{\rm light}$ from the g band.

Properties from galaxy catalogs—We then supplement the host galaxy properties from the catalogs of galaxies. During this process we match galaxies with SN hosts both by coordinates with a 3″ precision and by names.

For the galaxies within the coverage of SDSS, we use the parameters derived from the SDSS spectrum and broadband photometrics. The MPA-JHU group provided the stellar mass M_*, SFR, and metallicity of SDSS DR8 galaxies by taking both spectrum and photometrics into account (Kauffmann et al. 2003). We use their results when available. However, they did not provide the results for galaxies later than DR8. The flexible stellar population synthesis (SPS) used the SPS method to estimate the galaxy properties for both DR8 and DR12 galaxies (Conroy et al. 2009). We use their results for those not available in the MPA-JHU catalog. Karachentsev et al. (2013)[11] collected the SFR values estimated from Hα and the FUV of galaxies in the Local Volume. Up to 2020 January 1, this includes 1212 galaxies. We calibrate the galaxy names to their SIMBAD IDs, and match the names to the OSC SN hosts. Similarly, the SFR and stellar mass M_* from Vaddi et al. (2016) as well as the age and metallicity from Terlevich & Forbes (2002) are appended to the OSC SN hosts.

For the galaxies within the coverage of SDSS, we use the Sérsic half-light radius $R_{50,\rm s}$ in the NASA-SDSS Atlas catalog (NSA)[12] when available, which photometered 640,000 SDSS galaxies within $z < 0.15$. For large galaxies, e.g., $R_{50} \sim 1'$–$1\overset{\circ}{.}5$, Jarrett et al. (2003) estimated the radii of the largest 656 galaxies with images from the Two Micron All Sky Survey, which also include the galaxies outside the coverage of SDSS. We use the J-band $R_{\rm e}$ in Jarrett et al. (2003) for large galaxies instead. In addition, some R_{50} of SLSN hosts are provided in Lunnan et al. (2015). Otherwise, we use the the half-light radius within the SDSS catalog[13] by matching the SN host galaxies with SDSS galaxies within 3″. In the SDSS catalog, the half-light radius is estimated from the r-band Petrosian half-light radius $R_{50,\rm petro}$ and the Petrosian 90% radius $R_{50,\rm petro}$ following $R_{50} = R_{50,\rm petro}/(1 - 8 \times 10^{-6}(R_{90,\rm petro}/R_{50,\rm petro})^{8.47})$ (Graham et al. 2005).

We also update the offset parameters from the literatures. Lunnan et al. (2015) calculated the projected $R_{\rm off}$ from HST images for SLSNe. Anderson et al. (2016) reported the projected $R_{\rm off}$ from SNe II to the nearest H II regions. Kelly & Kirshner (2012) provided the deprojected $r_{\rm off} = R_{\rm off}/R_{50}$ for SNe II and SNe Ibc. Although projected offsets and

[8] https://ned.ipac.caltech.edu/forms/gmd.html
[9] http://www.astronomy.ohio-state.edu/~assassin/sn_list.html
[10] http://www.rochesterastronomy.org/snimages/snredshiftall.html
[11] https://www.sao.ru/lv/lvgdb/introduction.php
[12] http://www.nsatlas.org
[13] http://www.sdss3.org/

Table 2
Sample Size for Each Parameter of LGRBs, SLSNe, SNe Ibc, SNe II, SNe Ia and SGRBs

Type	LGRBs	SLSNe	SNe Ibc	SNe II	SNe Ia	SGRBs
Total	371	195	1300	6137	13086	32
log z	349	190	1218	4099	12290	24
log SFR ($M_\odot$ yr^{-1})	200	93	309	1122	2337	20
log sSFR (Gyr^{-1})	92	93	302	1085	2317	19
log M_* ($M_\odot$)	98	93	376	1257	2658	22
[X/H]	131	28	340	1290	2650	9
log R_{50} (kpc)	126	25	574	1868	4837	22
log offset (kpc)	134	35	767	2403	4915	26
log offset (R_{50})	115	20	511	3041	3293	22
$F_{\rm light}$	97	16	101	190	163	18
Any host parameter	263	107	900	4251	7221	31
sSFR and M_*	92	93	300	1078	2317	19
All parameters	26	2	52	95	70	6
$z < 1$						
log z	91	167	1217	4099	12227	23
log SFR ($M_\odot$ yr^{-1})	64	81	306	1101	2304	19
log sSFR (Gyr^{-1})	49	81	300	1065	2286	18
log M_* ($M_\odot$)	53	81	373	1233	2597	19
[X/H]	42	28	337	1265	2589	9
log R_{50} (kpc)	48	19	564	1868	4828	16
log offset (kpc)	51	29	758	2403	4914	18
log offset (R_{50})	45	14	497	1623	3131	16
$F_{\rm light}$	32	10	101	190	163	13
Any host parameter	72	95	874	2829	7003	22
sSFR and M_*	49	81	298	1058	2286	18
All parameters	12	2	52	95	70	6

deprojected offsets are statistically consistent, they are different for specific objects. Since most offsets in the literature and catalogs are projected, we use these deprojected offsets only when projected offsets are not available. We also convert them to $r_{\rm off}$ when R_{50} is available in our catalog.

The sample sizes for SLSNe, SNe Ibc, SNe II, and SNe Ia with host galaxy properties are 107, 900, 4251, and 7221, respectively. To have a consistent z range as the FRB sample, we screen the samples with $z < 1$. This gives sample sizes of 95, 874, 2829, and 7003 for the four types, respectively. Most SNe Ibc, SNe II, and SNe Ia have $z < 1$. The excluded objects are mostly those without redshift information.

The sample size for each parameter for each type of stellar transient is presented in Table 2.

3. Multivariate Comparison

We would like to perform a comparative study of the host galaxy properties between FRBs and other stellar transients. Since multiple parameters are involved, multivariate analysis methods are needed. We perform two tests. First, taking all the FRBs as a whole sample, we compare it with other samples using the multivariate Kolmogorov–Smirnov (KS) test. Second, we also compare each individual FRB with other samples to see which type it most likely belongs to. For easy understanding, we use the naive Bayes method to test individual FRBs in the FRB sample to see how they may be consistent with various types of stellar transients. We try to classify LGRBs, SLSNe, SNe Ib/Ic, SNe II, SNe Ia, and SGRBs with their host galaxy properties using the naive Bayes method and then apply the same method to each FRB. Galaxies evolve with redshift, and the FRBs in our sample all have redshift $z < 1$, so to enable a direct comparison, in the following we compare the FRBs with the transients with redshifts $z < 1$ only.

3.1. Multivariate KS Test

3.1.1. Method

The classical KS test compares the cumulative distribution function (CDF) of two distributions $P(<x)$ and $P(<x')$, which could be one data sample and one model sample, or two data samples. The largest distance between the two CDFs is defined as $D_{\rm KS} = \max(P(<x) - P(<x'))$, representing the difference between the two distributions x and x'. The distribution of $D_{\rm KS}$ is free from the distribution of x and x' and independent of the direction of data ordering, i.e., $D_{\rm KS}$ calculated from $P(<x)$ is the same as that calculated from $P(>x)$. This method is widely applied in defining the goodness of a fit or comparing two samples.

The key problem in generalizing the classical KS test to multiple dimensions is the direction of the data ordering. Peacock (1983) suggested using the maximum absolute difference between the two samples $D_{\rm DKS}$ when all possible directions along the axes are considered. For a two-dimensional problem, the difference $D_{\rm DKS}$ values are calculated for four quadrants of n^2 origins,

$$\begin{cases} (x < X_i,\ y < Y_j) \\ (x < X_i,\ y > Y_j) \\ (x > X_i,\ y < Y_j) \\ (x > X_i,\ y > Y_j) \end{cases}, \quad (i, j = 1, \ldots, n)$$

for all possible i and j values. Here n is the sample size, and the method applies to comparison of a data sample with a model.

Table 3
Multivariate KS Test Results

	M_* and sSFR			M_*, sSFR, $R_{\rm off}$			M_*, sSFR, R_{50}, $R_{\rm off}$, $F_{\rm light}$		
Name FRB	No. 7	$D_{\rm DKS}$	$P_{\rm DKS}$	No. 6	$D_{\rm DKS}$	$P_{\rm DKS}$	No. 2	$D_{\rm DKS}$	$P_{\rm DKS}$
LGRB	49	0.62	0.02	38	0.66	0.03	17	0.49	0.99
SLSNe	81	0.72	0.002	16	0.76	0.01	9	0.78	0.28
SN Ibc	298	0.38	0.68	250	0.41	0.85	55	0.70	0.95
SN II	1058	0.43	0.56	919	0.46	0.79	98	0.76	0.92
SN Ia	2286	0.46	0.42	1815	0.52	0.53	74	0.93	0.30
SGRB	18	0.29	0.81	16	0.36	0.80	11	0.64	0.76

$D_{\rm DKS}$ is confirmed to be efficient for correlated samples. For D dimensions, the number of quadrants to be calculated would be D^2n^D, which is computationally expensive for dimensions larger than 2 and/or $n > 100$.

Fasano & Franceschini (1987, hereafter FF87) proposed to use a simpler and faster method. For a two-dimensional problem, the difference $D_{\rm DKS}$ is calculated for four quadrants of n origins,

$$\begin{cases}(x < X_i,\ y < Y_i)\\ (x < X_i,\ y > Y_i)\\ (x > X_i,\ y < Y_i)\\ (x > X_i,\ y > Y_i)\end{cases}, \quad (i = 1, \ldots, n).$$

This method is proved not to compromise the power of the test. With this method, only D^2n quadrants should be considered for a D-dimensional comparison of size n, which is much more efficient than the method of Peacock (1983).

Moreover, FF87 generalized the method to two-sample multi-dimensional KS tests by proposing to use the average $\bar{D}_{\rm DKS}$ of the two $D_{\rm DKS}$ estimated according to the data sample 1 and sample 2. We use the two-sample method of FF87 in our analysis. However, the two-sample test in FF87 requires that the correlations among parameters are similar to each other in the two samples in order to use the probability P distribution presented in their paper. This may not be the case in our problem. We thus estimate the null probability P with Monte Carlo simulations. Since our FRB sample is much smaller than our stellar transient samples, in each trial we randomly extract the transient samples to have the same number of events as FRBs and calculate $D_{\rm mcDKS}$. We calculate $D_{\rm mcDKS}$ 1000 times and obtain the distribution of $D_{\rm mcDKS}$. The null probability $P_{\rm DKS}$ between the FRB host galaxy sample and the transient host galaxy samples is estimated by interpolating $D_{\rm DKS}$ in the simulated $D_{\rm mcDKS}$ distribution. Notice that such $P_{\rm DKS}$ values from this MC simulation may have large uncertainties when both the FRB sample and the transient sample are small.

3.1.2. Results for Galactic-scale Parameters: log M_* and log sSFR

The most common parameters available for transient host galaxies are stellar mass log M_* and log sSFR, regardless of whether the transients are well located on the sub-galactic scale. Thus, log M_* and log sSFR present the largest samples, both for FRBs and for other stellar transients. Seven FRB host galaxies have the information for log M_* and log sSFR. The numbers for each type transient with both log M_* and log sSFR are listed in the second column of Table 3. The FRBs (stars) are compared with various stellar transients in the log M_*–log sSFR plane in Figure 1. The stellar transient hosts and SDSS galaxies are presented as solid and dotted contours, with 1σ (68%) and 3σ (99.7%) confidence levels, respectively. The 1σ contours seem to occupy three regions in the log sSFR−log M_* diagram. (1) $7 <$ log $M_* < 10.5$ and $-1 <$ log sSFR < 1: LGRB (magenta) and SLSNe (orange) hosts occupy the strongest star formation region, while SLSN hosts have smaller stellar mass log M_* than LGRB hosts. (2) $8.5 <$ log $M_* < 11.5$ and $-3 <$ log sSFR < 0: SN Ibc (green) and SN II (dark green) hosts reside in the middle region in the log sSFR–log M_* plane. This region also contains the star-forming galaxy of SDSS and SN Ia (cyan) hosts. (3) $10 <$ log $M_* < 12$ and log sSFR < -2: There are also passive galaxy components in SN Ia hosts and SDSS (gray) galaxies. SGRB (blue) hosts occupy all three regions in the log sSFR−log M_* diagram. For FRBs, the host of FRB 121102 is located in the region with the smallest stellar mass and strongest star formation. The hosts of FRB 181112, FRB 190102, and FRB 190608 reside in the middle region. The hosts of FRB 180924, FRB 190523, and FRB 180916.J0158+65 are in the joint region between the star formation galaxies and the passive galaxy component of SDSS galaxies, SN Ia hosts, and SGRB

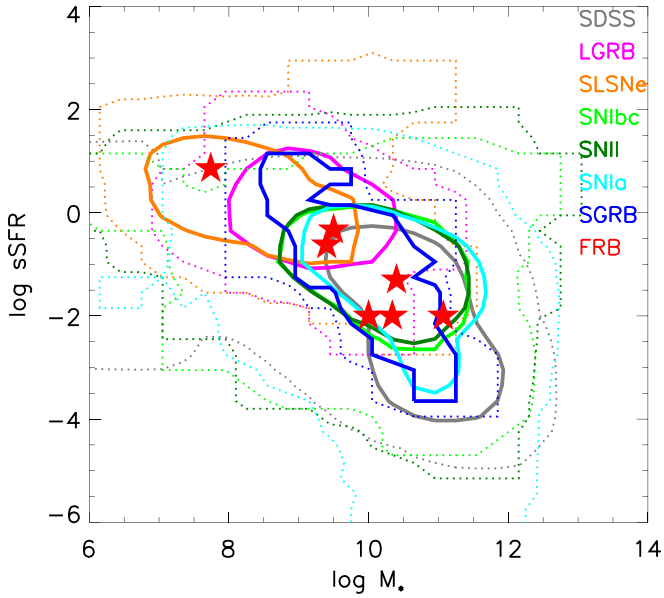

Figure 1. Comparison of FRB hosts (stars) with other stellar transients, as well as SDSS galaxies. The solid lines and dotted lines represent 1σ and 3σ regions of each stellar transient.

Table 4
Fitting Results of Each Parameter for All Parameters

	log SFR ($M_\odot$ yr^{-1})		log sSFR (Gyr^{-1})		log M_* ($M_\odot$)		[X/H]	
	$\mu \pm \sigma$	D_{KS}/P_{KS}	$\mu \pm \sigma$	D_{KS}/P_{KS}	$\mu \pm \sigma$	D_{KS}/P_{KS}	$\mu \pm \sigma$	D_{KS}/P_{KS}
LGRB	0.17 ± 0.81	0.09/0.69	0.01 ± 0.70	0.10/0.63	9.14 ± 0.68	0.06/0.99	-0.28 ± 0.28	0.10/0.78
SLSNe	-0.46 ± 0.82	0.05/0.98	0.29 ± 0.78	0.07/0.86	8.43 ± 0.96	0.10/0.34	-0.27 ± 0.44	0.14/0.61
SN Ibc	-0.27 ± 0.92	0.08/0.03	-1.22 ± 0.88	0.08/0.05	10.14 ± 0.87	0.09/0.01	0.02 ± 0.34	0.11/0.00
SN II	-0.12 ± 0.91	0.06/0.00	-1.19 ± 0.92	0.10/0.00	10.14 ± 0.81	0.07/0.00	-0.02 ± 0.36	0.12/0.00
SN Ia	-0.10 ± 0.98	0.10/0.00	-1.52 ± 1.16	0.13/0.00	10.50 ± 0.73	0.07/0.00	0.03 ± 0.37	0.12/0.00
SGRB	-0.04 ± 0.88	0.11/0.96	-1.06 ± 1.30	0.10/0.99	9.93 ± 0.79	0.11/0.96	-0.03 ± 0.16	0.19/0.87
FRB	-0.14 ± 0.45	0.26/0.68	-1.06 ± 1.09	0.24/0.77	9.78 ± 1.06	0.22/0.85	-0.31 ± 0.28	0.21/0.96
	log R_{50} (kpc)		log offset (kpc)		log offset (R_{50})		F_{light}	
	$\mu \pm \sigma$	D_{KS}/P_{KS}	$\mu \pm \sigma$	D_{KS}/P_{KS}	$\mu \pm \sigma$	D_{KS}/P_{KS}	$\mu \pm \sigma$	D_{KS}/P_{KS}
LGRB	0.30 ± 0.35	0.11/0.62	0.16 ± 0.61	0.11/0.60	-0.16 ± 0.40	0.09/0.83	2.62[a]	0.11/0.82
SLSNe	0.19 ± 0.50	0.17/0.60	0.47 ± 0.81	0.11/0.84	-0.14 ± 0.28	0.14/0.92	0.66 ± 0.27	0.13/0.99
SN Ibc	0.64 ± 0.39	0.10/0.00	0.55 ± 0.49	0.08/0.00	-0.14 ± 0.42	0.09/0.00	0.39 ± 1.09	0.35/0.00
SN II	0.66 ± 0.38	0.11/0.00	0.56 ± 0.48	0.07/0.00	-0.12 ± 0.46	0.09/0.00	0.45 ± 0.30	0.06/0.39
SN Ia	0.70 ± 0.31	0.07/0.00	0.60 ± 0.52	0.05/0.00	-0.12 ± 0.49	0.05/0.00	-1.53[a]	0.16/0.00
SGRB	0.62 ± 0.29	0.19/0.60	0.96 ± 0.49	0.16/0.70	0.30 ± 0.44	0.08/1.00	-4.35[a]	0.46/0.00
FRB	0.48 ± 0.22	0.24/0.91	0.61 ± 0.50	0.14/0.99	-0.11 ± 0.29	0.20/0.97	...	...

Note.
[a] For F_{light}, this is the index γ of the exponential distribution.

hosts. All FRB hosts except that for FRB 121102 are consistent with the hosts of SNe Ibc, SNe II, SNe Ia, and SGRBs within the 68% region.

We perform a two-dimensional KS test between FRBs and other transients in the log M_*–log sSFR space. D_{2KS} and the null probability values are presented in the third and fourth columns of Table 3. It turns out that the whole FRB sample rejects the origin similar to LGRBs and SLSNe at a significance level of 0.02, while other origins similar to SN Ibc, SN II, SN Ia, and SGRBs are still consistent with the FRB sample. Although the SGRB sample is small and the relation between its D_{DKS} and P_{DKS} has significant uncertainties, D_{DKS} of SGRBs is the smallest among all the transients, indicating similarity or more consistency of FRBs with SGRBs.

We also examine the differences among different types of transients in the log M_*–log SFR space (i.e., sSFR is replaced by SFR). The results are similar: that the FRB hosts and LGRB/SLSN hosts are significantly different, suggesting that the FRB host galaxy as a whole disfavors the LGRB and SLSNe origin. Similarly, the FRB hosts are also consistent with those of other transients in the log M_*–log SFR space.

We note that different SFR indicators represents stars with different ages (Kennicutt & Evans 2012), which introduces uncertainties to the SFR and sSFR in our sample. Moreover, SFR indicators, including emission lines, UV and IR emission, are usually influenced by the emission from active galactic nuclei. Many FRBs, including FRB 190102, FRB 180924, and FRB 190608, are located in galaxies with active nuclei or LINER emissions (Bhandari et al. 2020). In these cases, the log SFR and log sSFR values should be considered as the upper limits. As a result, to compare their environments more accurately, sub-galactic parameters should be taken into account.

3.1.3. Results for Combined Galactic and Sub-galactic Parameters: log M_*, log sSFR, log R_{50}, log R_{off}, and F_{light}

The positions of the transients within their host galaxies also provide important and usually more accurate information about the origin of the transients. The offset is available for all nine FRBs. However, the positional uncertainty of FRB 181112 is larger than the size of the galaxy. We do not include it in our analysis here. Although the positional uncertainty of FRB 190523 is also large, its offset is even more significant. We thus keep it in the sample. There are six FRBs with log M_*, log sSFR, and log R_{off} in our analysis. We perform a three-dimensional KS test between these six FRBs and other transients in the log M_*–log sSFR–log R_{off} space. The results are presented in columns 5–7 of Table 3. The conclusion is similar to what we found in the previous section: the FRB hosts as a whole disfavor the LGRB and SNSL origin.

On the other hand, the offset is also controlled by the size R_{50} and the gravitational well of the host. Also, due to the irregularity of some hosts, such as the host of FRB 121102, F_{light} better represents the local environments of the transients (Fruchter et al. 2006; Anderson et al. 2012). A more complete comparison of galactic and sub-galactic environments should include five parameters: log M_*, log sSFR, log R_{50}, log R_{off}, and F_{light}. The numbers of each type of transient with all five parameters are listed in the eighth column of Table 3, and the D_{2KS} values and the null probability values of the five-dimensional KS test between FRBs and other transients are presented in the ninth and tenth columns. However, due to the small size, the FRB sample does not show a significant difference with respect to any other type of stellar transient. A larger sample and/or a more detailed analysis of the FRB hosts may help to narrow down the preferred transients, if any, or suggest that FRBs are indeed consistent with a broad range of transient types.

3.2. Naive Bayes

It is possible that there might exist different subtypes of FRBs with distinct origins, so that different FRBs may fall into different distributions. While the multivariate KS test compares FRBs with other stellar transients as a whole sample, it cannot

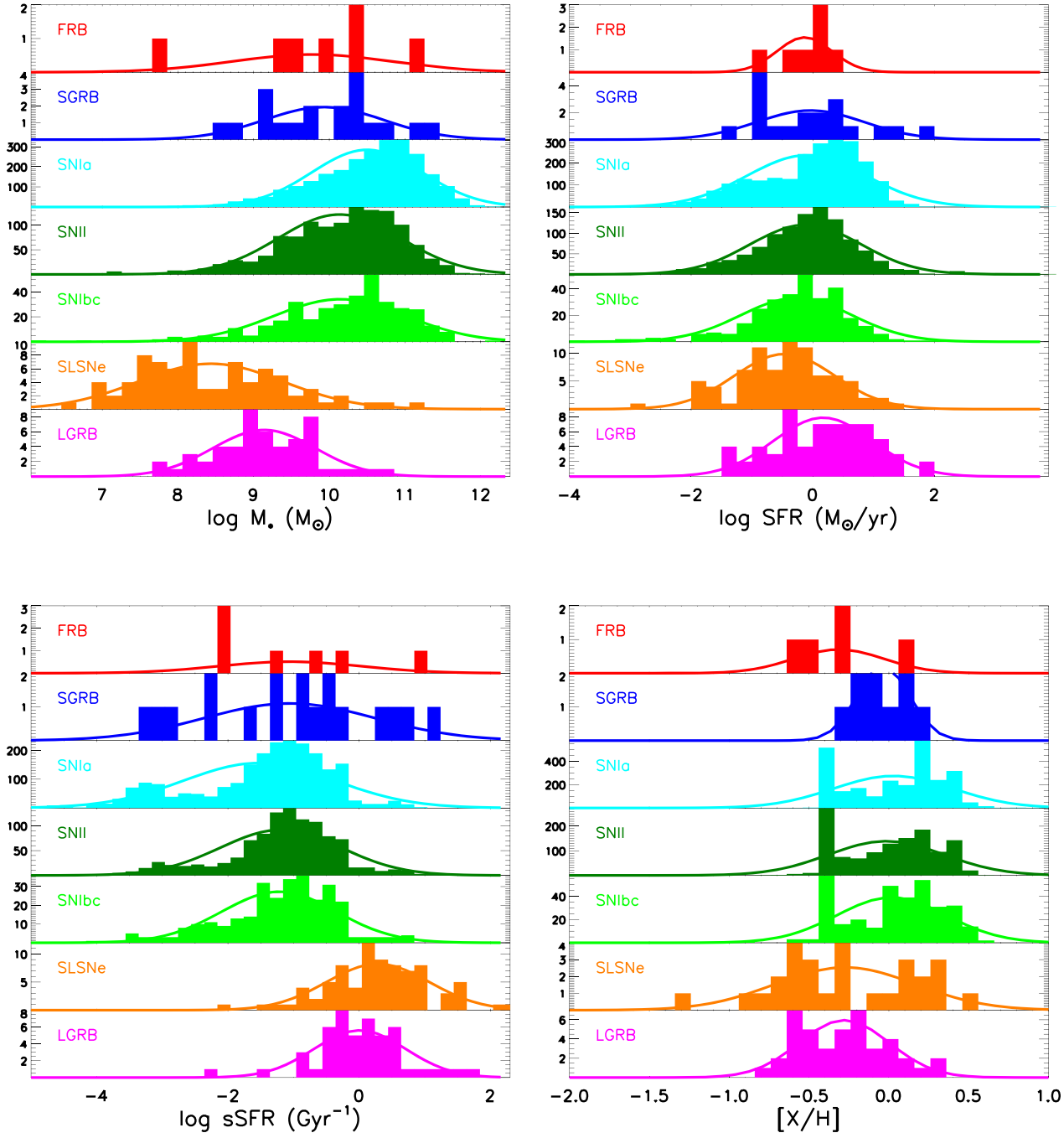

Figure 2. The distributions and fitting results of LGRBs (magenta), SLSNe (orange), SNe Ibc (green), SNe II (dark green), SNe Ia (cyan), SGRBs (blue), and FRBs (red).

test how individual FRBs fall into the distribution of a certain type of transient. We adopt the naive Bayes method to perform such a task.

3.2.1. Method

The naive Bayes method is a classification method based on the Bayes theorem and the assumption that parameters are not correlated, i.e.,

$$P(T|\{x\}) = \frac{P(\{x\}|T)P(T)}{P(\{x\})}, \quad (1)$$

$$P(\{x\}|T) = \prod_i P(x_i|T), \quad (2)$$

where $P(T|\{x\})$ is the posterior probability for one object with parameter set $\{x\}$ to have a type T, which could be LGRBs, SLSNe, SNe Ibc, SNe II, SNe Ia, or SGRBs; $P(\{x\}|T)$ is the likelihood for one object with a type T to have a parameter set $\{x\}$, $P(T)$ is the prior probability of one object being in type T, and $P(\{x\})$ is the probability of one object having a parameter set $\{x\}$. Although the assumption that parameters are uncorrelated is "naive," the results are amazingly good (Hand & Yu 2001; Broos et al. 2011).

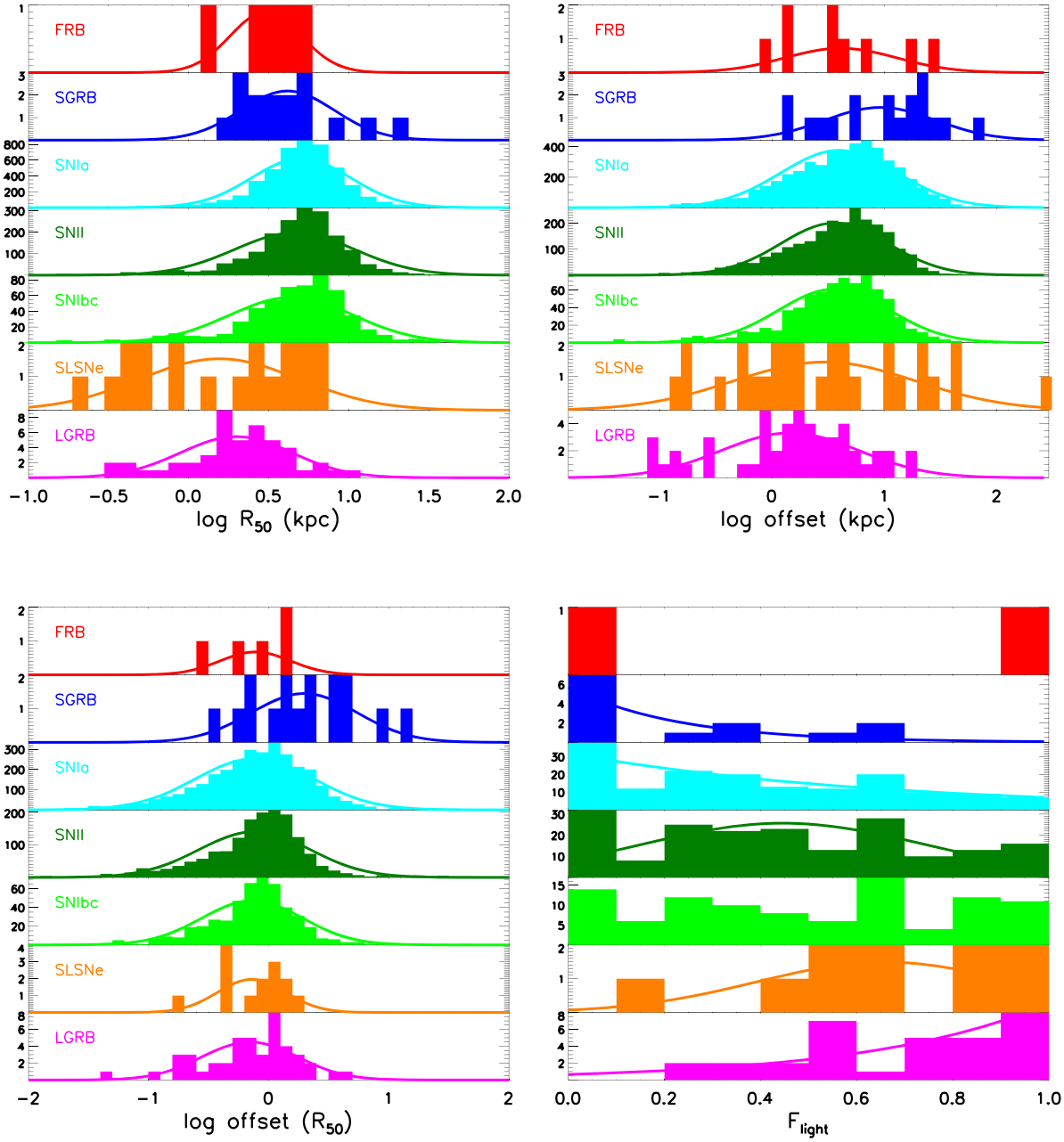

Figure 2. (Continued.)

The implementation of naive Bayes in our problem follows the following steps.

Estimate the likelihood $P(x_i|T)$ for each parameter x_i and type T with the known stellar transient samples.
Estimate the prior $P(T)$, usually by the size of the sample. However, for FRBs, we do not have any prior information about the preference to specific types. We thus use equal priors for all types of transients.
Calculate the posterior probability following Equation (2) for each type of transient T.
Normalize the posterior probability $P(T|\{x\})$ by requiring $\sum_j P(T_j|\{x\}) = 1$ for each FRB, where T_j stands for different transient types.
The type of the FRB is assigned to the one with the highest posterior probability.

We estimate the likelihood for each parameter x_i and type T, $P(x_i|T)$, with the observed sample in Section 2. Gaussian distributions are assumed for most parameters, while exponential distributions $P(x) \propto \exp(-x)$ are assumed for $F_{\rm light}$ for LGRBs, SNe Ia, and SGRBs. The fitting results are presented in Table 4 and Figure 2. The distribution of FRBs is also presented in red for comparison.

3.2.2. Results

The naive Bayes results for the stellar transients are presented in Figure 3. This shows the number of known LGRBs, SLSNe, SNe Ibc, SNe II, SNe Ia, and SGRBs classified as each type with naive Bayes. It turns out that most LGRBs, SLSNe, and SGRBs can be identified with their host galaxy properties. However, about half of the SNe Ibc, SNe II,

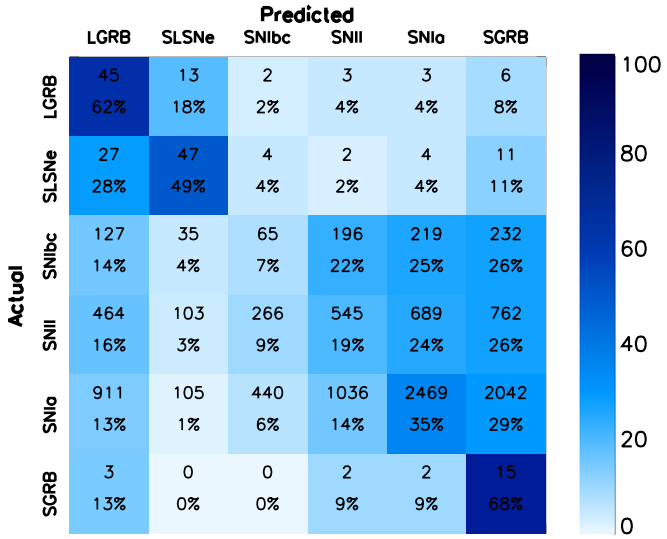

Figure 3. Confusion matrix of naive Bayes methods.

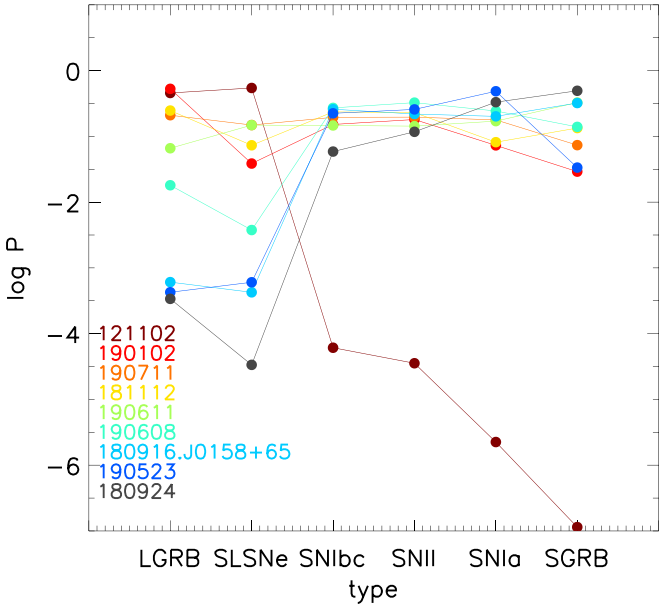

Figure 4. The probability of FRBs as various stellar transients.

Table 5
Probability of FRBs as Stellar Transients

FRB Name	LGRB	SLSNe	SN Ibc	SN II	SN Ia	SGRB
121102	0.46	0.54	6e−5	4e−5	2e−6	1e−7
180916. J0158+65	6e−4	4e−4	0.26	0.22	0.20	0.32
180924	3e−4	3e−5	0.06	0.12	0.33	0.49
181112	0.25	0.07	0.24	0.23	0.08	0.13
190102	0.53	0.04	0.15	0.18	0.07	0.03
190523	4e−4	6e−4	0.22	0.26	0.48	0.03
190608	0.02	4e−3	0.27	0.33	0.24	0.14
190611	0.07	0.15	0.15	0.14	0.17	0.33
190711	0.21	0.15	0.19	0.20	0.18	0.07

and SNe Ia may be misclassified as SGRBs, suggesting that the host galaxy properties of these transients are not that different from those of SGRBs.

We apply the same method to individual FRBs. The results are presented in Table 5 and Figure 4. The following conclusions can be drawn. The host of FRB 121102 has 90% probability of belonging to the SLSN sample and 10% probability of belonging to the LGRB sample, and its probabilities of belonging to SN Ibc, SN II, SN Ia, and SGRB samples are significantly smaller. FRB 180916.J0158+65 has a very low probability of belonging to the LGRB or SLSN samples, but is consistent with belonging to one of the SN Ibc, SN II, SN Ia, or SGRB samples. FRB 180924 also has a very low probability of belonging to the LGRB/SLSN sample but has a fairly high probability of belonging to SN Ia or SGRB samples. FRB 181112 has a reasonable probability of belonging to any sample, due to its mild SFR and log M_* and the lack of sub-galactic information. FRB 190523 also disfavors an LGRB/SLSN origin but is consistent with an SN Ibc, SN II, or SN Ia origin. Its consistency with the SGRB sample is marginal.

4. Conclusion and Discussion

In this paper, we compare the properties of FRB host galaxies with those of various stellar transients, including LGRBs, SLSNe, SNe Ibc, SNe II, SNe Ia, and SGRBs. Considering the FRBs with host galaxies as a whole, a multivariate KS test reveals that FRB hosts are not consistent with the hosts of LGRBs and SLSNe at a significance level of 0.02. Due to the small sample statistics, they are still consistent with the distribution of the hosts of all other transients. Comparing the FRBs hosts with the stellar transient hosts individually, we find that FRB 121102 tends to have a similar origin to LGRBs and SLSNe, while FRB 180924, FRB 190523, FRB 180916.J0158+65, and FRB 190608 are more similar to SNe Ibc, SNe II, SNe Ia, or SGRBs. FRB 190102, FRB 190711, FRB 181112, and FRB 190611 do not show obvious preference for any type.

The results in our study may shed light on the unknown energy source of FRBs. The first implication is that repeating FRBs and apparently non-repeating FRBs do not show a dichotomy in terms of host galaxy properties. In fact, two active repeaters, FRB 121102 (Spitler et al. 2016; Chatterjee et al. 2017; Marcote et al. 2017; Tendulkar et al. 2017) and FRB 180916.J0158+65 (CHIME/FRB Collaboration et al. 2019b; Marcote et al. 2020), show opposite host galaxy properties and cannot be grouped into the same category of host galaxy. Some apparently non-repeating FRBs, such as FRB 190608, share similar properties to FRB 180916, which is consistent with the speculation that most (or at least some) apparently non-repeating FRBs may be repeating ones (Lu & Piro 2019; Ravi 2019).

The leading FRB source model invokes magnetars as the power source to produce repeating bursts. There are two versions of this model. One version invokes rapidly spinning young magnetars that are produced in extreme stellar transients such as GRBs and SLSNe. The main motivation is that the host galaxy of FRB 121102 resembles those of LGRBs and SLSNe (Metzger et al. 2017; Nicholl et al. 2017; Wadiasingh & Timokhin 2019). The fact that the hosts of all other FRBs do not resemble that of FRB 121102 disfavors the simplest version of this proposal. A possible fix of this proposal is to introduce rapidly spinning magnetars born from binary neutron star (BNS) mergers (Margalit et al. 2019; Wang et al. 2020). In order to make this scenario work, one needs to require that

rapidly spinning magnetars made from BNS mergers should be much more abundant than those made from LGRBs and SLSNe. Comparing the event rate densities of BNS mergers, LGRBs, and SLSNe (e.g., Sun et al. 2015; Abbott et al. 2017; Nicholl et al. 2017), this may be possible if a significant fraction of BNS mergers leave behind stable neutron stars (e.g., Gao et al. 2016). However, if this fraction is very low, as required if GW170817 leaves behind a black hole (Margalit et al. 2019), the fast magnetar model may fail to explain the small fraction of LGRB/SLSN-like hosts in FRB samples. The second version of the magnetar model invokes emission (e.g., giant flares) from slowly rotating magnetars like the ones observed in the Galaxy (e.g., Popov & Postnov 2010; Katz 2014; Kulkarni et al. 2014). The births of these magnetars do not require extreme explosions such as GRBs and SLSNe (e.g., Beniamini et al. 2019). If this is the case, the host galaxy distribution may be more analogous to that of SNe II. All FRBs but FRB 121102 are consistent with this scenario (Figure 4). In order to interpret FRB 121102, the more extreme channel of forming rapid magnetars is still needed. So we conclude that the magnetar model would work only if both fast magnetars produced in extreme explosions and slow magnetars produced in regular channels (Beniamini et al. 2019) can produce FRBs. In any case, since the birth rate of these magnetars is very high (Beniamini et al. 2019), an additional factor is needed to select a small fraction of magnetars to produce FRBs (e.g., Ioka & Zhang 2020).

Some non-magnetar models may be accommodated by the data. The cosmic comb model (Zhang 2017) invokes a variety of possible donors to reshape the magnetosphere of neutron stars. These events can in principle occur in a variety of host galaxies with a variety of local environments. However, most other models are consistent with the FRBs apart from FRB 121102. The pre-merger BNS interaction model (Zhang 2020) would predict host galaxy type and local environments similar to those of SGRBs. Models invoking white dwarf mergers (Kashiyama et al. 2013) or white dwarf accretion (Gu et al. 2016) may have hosts similar to SNe Ia. The $\sim$16 days periodicity of FRB 180916.J0158+65 (Marcote et al. 2020) may require a binary system (e.g., Dai & Zhong 2020; Ioka & Zhang 2020; Katz 2020; Lyutikov et al. 2020, see also Beniamini et al. 2020). These systems may have a host galaxy or local environment similar to intermediate stellar populations.

The constraints on the FRB source models are limited by the small sample of FRBs with host galaxy observations. Continued localization campaigns of FRBs by ASKAP and other facilities will increase the sample of FRB hosts significantly in the coming years. On the other hand, the intrinsic degeneracy of the host galaxy properties among many stellar explosions (e.g., SNe Ib/c, SNe II, SGRBs) makes it difficult to identify the origin of FRBs based on the host galaxy properties alone. Additional information (e.g., multi-frequency counterparts, periodicity) is needed to eventually pin down the origin of FRBs.

We thank the anonymous referee for helpful suggestions and comments. Y.L. thanks Dongdong Shi, Qiang Yuan, and Jie Zheng for helpful discussion. Y.L. is supported by the KIAA-CAS Fellowship, which is jointly supported by Peking University and Chinese Academy of Sciences. Her work is also partially supported by the China Postdoctoral Science Foundation (No. 2018M631242).

Funding for SDSS-III has been provided by the Alfred P. Sloan Foundation, the Participating Institutions, the National Science Foundation, and the U.S. Department of Energy. The SDSS-III website is http://www.sdss3.org.

SDSS-III is managed by the Astrophysical Research Consortium for the Participating Institutions of the SDSS-III Collaboration including the University of Arizona, the Brazilian Participation Group, Brookhaven National Laboratory, University of Cambridge, University of Florida, the French Participation Group, the German Participation Group, the Instituto de Astrofisica de Canarias, the Michigan State/Notre Dame/JINA Participation Group, Johns Hopkins University, Lawrence Berkeley National Laboratory, Max Planck Institute for Astrophysics, New Mexico State University, New York University, Ohio State University, Pennsylvania State University, University of Portsmouth, Princeton University, the Spanish Participation Group, University of Tokyo, University of Utah, Vanderbilt University, University of Virginia, University of Washington, and Yale University.

ORCID iDs

Ye Li https://orcid.org/0000-0001-5931-2381
Bing Zhang https://orcid.org/0000-0002-9725-2524

References

Abbott, B. P., Abbott, R., Abbott, T. D., et al. 2017, PhRvL, 119, 161101
Ahumada, R., Allende Prieto, C., Almeida, A., et al. 2020, ApJS, 249, 3
Anderson, J. P., Gutiérrez, C. P., Dessart, L., et al. 2016, A&A, 589, A110
Anderson, J. P., Habergham, S. M., James, P. A., & Hamuy, M. 2012, MNRAS, 424, 1372
Anderson, J. P., James, P. A., Förster, F., et al. 2015a, MNRAS, 448, 732
Anderson, J. P., James, P. A., Habergham, S. M., Galbany, L., & Kuncarayakti, H. 2015b, PASA, 32, e019
Arnouts, S., Cristiani, S., Moscardini, L., et al. 1999, MNRAS, 310, 540
Asplund, M., Grevesse, N., Sauval, A. J., & Scott, P. 2009, ARA&A, 47, 481
Bannister, K. W., Deller, A. T., Phillips, C., et al. 2019, Sci, 365, 565
Bassa, C. G., Tendulkar, S. P., Adams, E. A. K., et al. 2017, ApJL, 843, L8
Beloborodov, A. M. 2017, ApJL, 843, L26
Beniamini, P., Hotokezaka, K., van der Horst, A., & Kouveliotou, C. 2019, MNRAS, 487, 1426
Beniamini, P., Wadiasingh, Z., & Metzger, B. D. 2020, MNRAS, 496, 3390
Berger, E. 2009, ApJ, 690, 231
Berger, E. 2014, ARA&A, 52, 43
Bhandari, S., Sadler, E. M., Prochaska, J. X., et al. 2020, ApJL, 895, L37
Blanchard, P. K., Berger, E., & Fong, W.-f. 2016, ApJ, 817, 144
Bloom, J. S., Kulkarni, S. R., & Djorgovski, S. G. 2002, AJ, 123, 1111
Boquien, M., Burgarella, D., Roehlly, Y., et al. 2019, A&A, 622, A103
Broos, P. S., Getman, K. V., Povich, M. S., et al. 2011, ApJS, 194, 4
Chatterjee, S., Law, C. J., Wharton, R. S., et al. 2017, Natur, 541, 58
CHIME/FRB Collaboration, Amiri, M., Bandura, K., et al. 2019a, Natur, 566, 235
CHIME/FRB Collaboration, Andersen, B. C., Bandura, K., et al. 2019b, ApJL, 885, L24
Chung, C., Yoon, S.-J., Lee, S.-Y., & Lee, Y.-W. 2013, ApJS, 204, 3
Conroy, C., Gunn, J. E., & White, M. 2009, ApJ, 699, 486
Cordes, J. M., & Chatterjee, S. 2019, ARA&A, 57, 417
Cucchiara, A., Fumagalli, M., Rafelski, M., et al. 2015, ApJ, 804, 51
Dai, Z. G., & Zhong, S. Q. 2020, ApJL, 895, L1
Dopita, M. A., Kewley, L. J., Sutherland, R. S., & Nicholls, D. C. 2016, Ap&SS, 361, 61
Draine, B. T. 2011, Physics of the Interstellar and Intergalactic Medium (Princeton, NJ: Princeton Univ. Press)
Fasano, G., & Franceschini, A. 1987, MNRAS, 225, 155
Fong, W., & Berger, E. 2013, ApJ, 776, 18
Fong, W., Berger, E., & Fox, D. B. 2010, ApJ, 708, 9
Fonseca, E., Andersen, B. C., Bhardwaj, M., et al. 2020, ApJL, 891, L6
Fruchter, A. S., Levan, A. J., Strolger, L., et al. 2006, Natur, 441, 463
Gao, H., Zhang, B., & Lü, H.-J. 2016, PhRvD, 93, 044065
Gogarten, S. M., Dalcanton, J. J., Williams, B. F., et al. 2009, ApJ, 691, 115

Graham, A. W., Driver, S. P., Petrosian, V., et al. 2005, AJ, 130, 1535
Graham, J. F. 2019, arXiv:1905.13197
Gu, W.-M., Dong, Y.-Z., Liu, T., Ma, R., & Wang, J. 2016, ApJL, 823, L28
Hand, D. J., & Yu, K. 2001, International Statistical Review, 69, 385
Ioka, K., & Zhang, B. 2020, ApJL, 893, L26
Japelj, J., Vergani, S. D., Salvaterra, R., et al. 2018, A&A, 617, A105
Jarrett, T. H., Chester, T., Cutri, R., Schneider, S. E., & Huchra, J. P. 2003, AJ, 125, 525
Kang, Y., Kim, Y.-L., Lim, D., Chung, C., & Lee, Y.-W. 2016, ApJS, 223, 7
Kang, Y., Lee, Y.-W., Kim, Y.-L., Chung, C., & Ree, C. H. 2020, ApJ, 889, 8
Karachentsev, I. D., Makarov, D. I., & Kaisina, E. I. 2013, AJ, 145, 101
Kashiyama, K., Ioka, K., & Mészáros, P. 2013, ApJL, 776, L39
Katz, J. I. 2014, PhRvD, 89, 103009
Katz, J. I. 2016, ApJ, 826, 226
Katz, J. I. 2020, MNRAS, 494, L64
Kauffmann, G., Heckman, T. M., White, S. D. M., et al. 2003, MNRAS, 341, 33
Kelly, P. L., & Kirshner, R. P. 2012, ApJ, 759, 107
Kelly, P. L., Kirshner, R. P., & Pahre, M. 2008, ApJ, 687, 1201
Kennicutt, R. C., & Evans, N. J. 2012, ARA&A, 50, 531
Kewley, L. J., & Dopita, M. A. 2002, ApJS, 142, 35
Kewley, L. J., & Ellison, S. L. 2008, ApJ, 681, 1183
Kim, Y.-L., Smith, M., Sullivan, M., & Lee, Y.-W. 2018, ApJ, 854, 24
Kobulnicky, H. A., & Kewley, L. J. 2004, ApJ, 617, 240
Kokubo, M., Mitsuda, K., Sugai, H., et al. 2017, ApJ, 844, 95
Krühler, T., Malesani, D., Fynbo, J. P. U., et al. 2015, A&A, 581, A125
Kulkarni, S. R., Ofek, E. O., Neill, J. D., Zheng, Z., & Juric, M. 2014, ApJ, 797, 70
Kumar, P., Shannon, R. M., Osłowski, S., et al. 2019, ApJL, 887, L30
Leibler, C. N., & Berger, E. 2010, ApJ, 725, 1202
Li, Y., Zhang, B., & Lü, H.-J. 2016, ApJS, 227, 7
Li, Y., Zhang, B., Nagamine, K., & Shi, J. 2019, ApJL, 884, L26
Li, Y., Zhang, B., & Yuan, Q. 2020, ApJ, 897, 154
Lorimer, D. R., Bailes, M., McLaughlin, M. A., Narkevic, D. J., & Crawford, F. 2007, Sci, 318, 777
Lu, W., & Piro, A. L. 2019, ApJ, 883, 40
Lunnan, R., Chornock, R., Berger, E., et al. 2015, ApJ, 804, 90
Luo, R., Lee, K. J., Men, Y. P., & Zhang, B. 2020, Natur, submitted
Lyutikov, M., Barkov, M. V., & Giannios, D. 2020, ApJL, 893, L39
Macquart, J. P., Prochaska, J. X., McQuinn, M., et al. 2020, Natur, 581, 391
Marcote, B., Nimmo, K., Hessels, J. W. T., et al. 2020, Natur, 577, 190
Marcote, B., Paragi, Z., Hessels, J. W. T., et al. 2017, ApJL, 834, L8
Margalit, B., Berger, E., & Metzger, B. D. 2019, ApJ, 886, 110
Metzger, B. D., Berger, E., & Margalit, B. 2017, ApJ, 841, 14
Murase, K., Kashiyama, K., & Mészáros, P. 2016, MNRAS, 461, 1498
Nicholl, M., Williams, P. K. G., Berger, E., et al. 2017, ApJ, 843, 84
Peacock, J. A. 1983, MNRAS, 202, 615
Perley, D. A., Quimby, R. M., Yan, L., et al. 2016, ApJ, 830, 13
Petroff, E., Barr, E. D., Jameson, A., et al. 2016, PASA, 33, e045
Petroff, E., Hessels, J. W. T., & Lorimer, D. R. 2019, A&ARv, 27, 4
Pettini, M., & Pagel, B. E. J. 2004, MNRAS, 348, L59
Planck Collaboration, Ade, P. A. R., Aghanim, N., et al. 2016, A&A, 594, A13
Platts, E., Weltman, A., Walters, A., et al. 2019, PhR, 821, 1
Popov, S. B., & Postnov, K. A. 2010, in Conf. Proc. Evolution of Cosmic Objects through their Physical Activity, ed. H. A. Harutyunian, A. M. Mickaelian, & Y. Terzian (Yerevan: "Gitutyun" Publishing House of NAS RA), 129
Prochaska, J. X., Macquart, J.-P., McQuinn, M., et al. 2019, Sci, 366, 231
Ravi, V. 2019, NatAs, 3, 928
Ravi, V., Catha, M., D'Addario, L., et al. 2019, Natur, 572, 352
Sako, M., Bassett, B., Becker, A. C., et al. 2018, PASP, 130, 064002
Savaglio, S., Glazebrook, K., & Le Borgne, D. 2009, ApJ, 691, 182
Schady, P., Eldridge, J. J., Anderson, J., et al. 2019, MNRAS, 490, 4515
Scholz, P., Spitler, L. G., Hessels, J. W. T., et al. 2016, ApJ, 833, 177
Schulze, S., Krühler, T., Leloudas, G., et al. 2018, MNRAS, 473, 1258
Spitler, L. G., Scholz, P., Hessels, J. W. T., et al. 2016, Natur, 531, 202
Sun, H., Zhang, B., & Li, Z. 2015, ApJ, 812, 33
Taggart, K., & Perley, D. 2019, arXiv:1911.09112
Tendulkar, S. P., Bassa, C. G., Cordes, J. M., et al. 2017, ApJL, 834, L7
Terlevich, A. I., & Forbes, D. A. 2002, MNRAS, 330, 547
Totani, T. 2013, PASJ, 65, L12
Vaddi, S., O'Dea, C. P., Baum, S. A., et al. 2016, ApJ, 818, 182
Wadiasingh, Z., & Timokhin, A. 2019, ApJ, 879, 4
Wainwright, C., Berger, E., & Penprase, B. E. 2007, ApJ, 657, 367
Wang, F. Y., Wang, Y. Y., Yang, Y.-P., et al. 2020, ApJ, 891, 72
Zhang, B. 2017, ApJL, 836, L32
Zhang, B. 2020, ApJL, 890, L24